Journal of Marine Research, 54, 1207–1227, 1996

Modeling ^{210}Pb-derived mixing activity in ocean margin sediments: Diffusive versus nonlocal mixing

by Karline Soetaert[1], Peter M. J. Herman[1], Jack J. Middelburg[1], C. Heip[1], Henko S. deStigter[2], Tjeerd C. E. van Weering[2], E. Epping[2,3] and W. Helder[2]

ABSTRACT

The influence of sediment mixing on activity versus depth profiles of the radionuclide ^{210}Pb in the upper 20 cm of the sediments has been investigated along a depth transect (208 m–4500 m, 17 stations) in the OMEX study area (Goban Spur, NE Atlantic Ocean). A hierarchical family of bioturbation/nonlocal exchange models was derived. Each member of the hierarchy includes all processes of the previous model, and adds a one- or two-parameter process. The significance of the additional parameters is tested using a one-tailed *F*-test. It was found that (1) in five cases there is a significant improvement when direct injection of part of the flux into deeper sediment layers (nonlocal exchange) is added to the diffusive mixing model. (2) In these five cases, the best model required only two additional parameters, compared to the diffusive mixing model. More elaborate models, including additional parameters did not result in a significantly better fit. (3) In four cases, the inclusion of diffusive mixing (bioturbation) to an advection/decay model does not result in a significant better fit of modeled versus measured ^{210}Pb activity-depth profiles. Using the simplest nonlocal exchange model, the amount of particulates that are directly injected at depth into the sediment was estimated and compared with the amount incorporated at the sediment surface. Along the OMEX transect, between 8–86% of the total flux enters the sediment by nonlocal exchange rather than by mere bioturbation/advection at the sediment surface. The importance of nonlocal exchange decreases with increasing water depth. To allow comparison with other measurements, we have also calculated the diffusive mixing coefficient using the classical bioturbation model. The sediments in the OMEX area have low bioturbation coefficients, especially at the deeper sites. Finally our models have also been used to reproduce and to explore some aberrant ^{210}Pb profiles reported in the literature.

1. Introduction

Particulate matter arriving at the seafloor may enter the sedimentary column either through physical processes or by the activities of organisms. Because transport processes may have important consequences for diagenetic pathways (Aller, 1990), it is important to understand and quantify the way these particles enter the sediment and are moved around.

1. Netherlands Institute of Ecology, Centre for Estuarine and Coastal Research, Vierstraat 28, 4401-EA Yerseke, The Netherlands.
2. Netherlands Institute for Sea Research, P.O. Box 59, 1790 AB DenBurg, Texel, The Netherlands.
3. Present address: Max Planck Institute For Marine Microbiology, Celsiusstr. 1, D-28359 Bremen, Germany.

If sediment reworking consists of a large number of small events, the effect appears as diffusive mixing (Boudreau, 1986a), and this activity can be quantified as a bioturbation coefficient (Db). This diffusive mixing coefficient is usually estimated by modeling sediment-depth profiles of particle-bound radioactive tracers with ecologically significant half-lives. The existence of subsurface maxima in such sediment-depth profiles is not consistent with diffusional mixing and is usually attributed to other effects, e.g. a fluctuating source, the infilling of a large burrow, or a species that places surface material at depth (nonlocal exchange, Boudreau, 1986b). Such phenomena complicate the calculation of diffusive bioturbation rates, hence the data corresponding to the subsurface maxima are often ignored (e.g. Legeleux *et al.,* 1994; Thomson *et al.,* 1993) or, when included in the analysis, the obtained rates of bioturbative mixing may be seriously overestimated (Smith *et al.,* 1986).

Only few investigators have applied a nonlocal exchange model to sediment mixing (Boudreau, 1986b; Boudreau and Imboden, 1987; Buffoni *et al.,* 1992; Smith *et al.,* 1986) and until now the various models have not been consistently compared, nor has their capability to actually reproduce activity versus depth profiles of radionuclides been demonstrated.

The radioactive tracer ^{210}Pb is strongly associated with particulate matter, hence its redistribution in the sediment mainly depends on its supply at the interface, *in situ* production from sedimentary U via ^{226}Ra decay, sediment accumulation and physical or biological mixing. As its mean half-life (22.4 yr) is of ecological and biogeochemical significance, profiles of this isotope have been extensively used to estimate sedimentation rates (e.g. Nittrouer *et al.,* 1983; DeMaster *et al.,* 1994), biodiffusion coefficients (e.g. Kim and Burnett, 1988; Anderson *et al.,* 1994; Boudreau, 1994) and mixed-layer depths (Boudreau, 1994).

In this paper we describe a family of diffusive mixing/nonlocal exchange models and demonstrate their applicability and limitations in reproducing ^{210}Pb profiles of 17 stations along the ocean margin in the Goban Spur area (NE Atlantic). *F*-statistics are used to test what elaboration of the models is necessary to significantly improve the fit of observed versus modeled activities.

2. Material and methods

a. Sampling and measurements

This work was performed in the framework of the MASTII Ocean Margin Exchange (OMEX) project, which aims at a better understanding of exchange processes along the ocean margin. The sediment cores were collected in the Goban Spur area (NE Atlantic) during two OMEX cruises in different seasons (October 1993, May–June 1994) with R.V. *Pelagia* and R.V. *Darwin.* Five stations were sampled twice (Stations A/D86-1, I/D86-2, B/D86-3, II/D86-4 and F/D86-5); the other stations were sampled during only one cruise

Table 1. Sampling location and depth of the various stations, arranged according to water depth.

Station	Date	Depth m	Latitude	Longitude
A	October 93	208	049° 29′N	011° 08′W
D86-01	May–June 94	208	049° 29′N	011° 08′W
I	October 93	670	049° 25′N	011° 32′W
D86-02	May–June 94	670	049° 25′N	011° 32′W
B	October 93	1034	049° 22′N	011° 48′W
D86-03	May–June 94	1034	049° 22′N	011° 48′W
D86-11	May–June 94	1120	049° 05′N	011° 44′W
D86-08	May–June 94	1175	049° 14′N	012° 31′W
II	October 93	1425	049° 11′N	012° 49′W
D86-04	May–June 94	1425	049° 11′N	012° 50′W
C	October 93	1961	049° 10′N	012° 59′W
F	October 93	2182	049° 09′N	013° 05′W
D86-09	May–June 94	2218	048° 51′N	012° 45′W
D86-05	May–June 94	2250	049° 10′N	013° 05′W
D86-10	May–June 94	2294	048° 52′N	012° 39′W
D86-06	May–June 94	3675	049° 05′N	013° 26′W
D86-07	May–June 94	4500	049° 02′N	013° 42′W

(Table 1; Fig. 1). Station depths ranged from 208 to 4500 m. Sediments were collected by a modified, cylindrical (50 cm) boxcorer with a closing lid on top, that obtained undisturbed surface sediments. The sedimentation rates at these sites, which were determined using stratigraphic techniques on samples from the same box corers and (for some) confirmed by ^{14}C AMS dating are in the order of 1–6 cm $\cdot$ kyr^{-1}; only one station (station II, D86-04) had a lower sedimentation rate (0.1 cm $\cdot$ kyr^{-1}) (van Weering and de Stigter, 1995). ^{210}Pb total activities were determined indirectly by measuring its alpha granddaughter ^{210}Po, following the procedure outlined by van Weering *et al.* (1987). Measured dry weight/wet volume ratios were subsequently used to convert the activities to volumetric units. Because no measurements for the supported activity were available, it was estimated as an additional parameter in the nonlinear estimation routine.

b. The model and its solution

Sediment mixing occurs at various time and space scales. Given a large number of mixing events, small-scale mixing can be well described as a diffusion-like process, whereas a nonlocal exchange approach is more appropriate for mixing at larger scales. Boudreau and Imboden (1987) consider depth-independent diffusion and continuous nonlocal mixing as two reasonable endmember possibilities for sediment mixing. We will follow their approach since, having only ^{210}Pb measurements, it is probably not possible to determine if and how bioturbation coefficients change with depth (Boudreau, 1986a) or to distinguish between single-event versus continuous nonlocal mixing (Smith *et al.*, 1986).

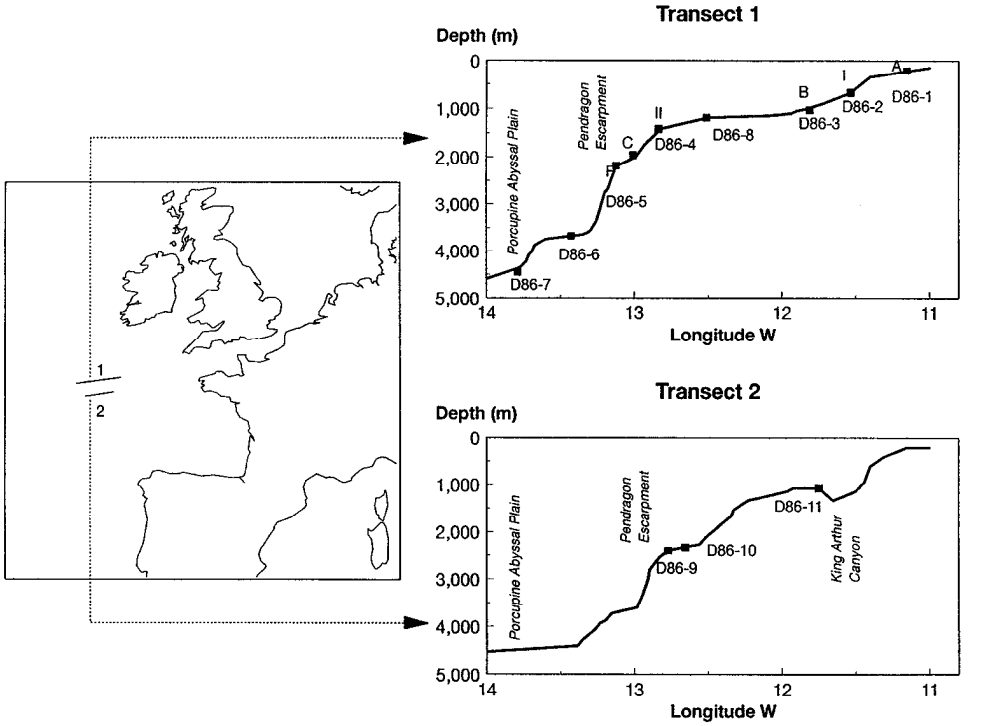

Figure 1. Location of the Goban Spur transects 1 and 2 (left) and the stations (right). Stations indicated as D86-.. were sampled in May–June 1994; the others were sampled in October 1993.

At steady state (constant supply of ^{210}Pb), continuous nonlocal mixing and no porosity gradient, the concentration of total ^{210}Pb in some layer i (C_i) subjected to advection, mixing, production and radioactive decay can be represented by (Berner, 1980):

$$Db\frac{d^2C_i}{dx^2} - w\frac{dC_i}{dx} - \lambda C_i - rC_i + Q_i + Sp = 0 \tag{1}$$

where x denotes depth into the sediment (cm, increasing downward), Db is the (constant) sediment diffusive mixing coefficient (cm^2 yr^{-1}), w is the sedimentation rate (cm yr^{-1}), λ is the decay rate (yr^{-1}), r is a first-order ingestion rate (yr^{-1}), Q_i and Sp (constants) denote either a zero-order production or consumption term. In our case, C_i is in dpm cm^{-3} bulk sediment, Q_i is the nonlocal exchange input to layer i; Sp is the production of supported ^{210}Pb, which is equal for all layers.

The solution of this equation is of the form (when $Db > 0$):

$$c_i(x) = A_i e^{\theta_1 \cdot x} + E_i e^{\theta_2 \cdot x} + \frac{(Q_i + Sp)}{(\lambda + r)}$$

where

$$\theta_1 = \frac{w - \sqrt{w^2 + 4(\lambda + r)Db}}{2Db} \quad \text{and} \quad \theta_2 = \frac{w + \sqrt{w^2 + 4(\lambda + r)Db}}{2Db}$$

and A_i and E_i are integration constants.

In case Db, Q_i and $r = 0$ (i.e. the advective case), the solution to the equation is:

$$c_i(x) = A_i \cdot e^{-(\lambda/w)\cdot x} + \frac{Sp}{\lambda}.$$

c. The family of models that was tested

The diagenetic equations and boundary conditions of the various models that were used in this work are depicted in Figure 2. The parameters to fit in each case are shown in Table 2. The boundary conditions (defined in the inset of Fig. 2) determine the integration constants (exemplified for model 4b in the Appendix). They are: a flux boundary at the sediment-water interface (B0, B1), continuity of activity (B2) and continuity of flux (B3, B4) in between layers, and the no-gradient boundary (B5) at depth. Notice that if both B2 and B3 are valid, and since Db and w are constant, the continuity of flux (B3) can be replaced by the continuity of gradient boundary which is more easy to implement. Also, some investigators prefer to express the boundary condition at the sediment-water interface as a concentration boundary rather than a flux boundary (e.g. Smith *et al.,* 1986).

Model (1). The simplest model has no mixing by organisms or other processes (Db, r and Q_i in Eq. (1) are 0). The distribution of ^{210}Pb in the sediments is then influenced only by the flux, sedimentation (rate w), decay (rate λ) and supported activity. There is only one layer with a flux boundary at the sediment-water interface (B0).

The sedimentation rate and the decay rate of ^{210}Pb being known (0.031 yr^{-1}), the least squares fit algorithm has to find the best value of the (unknown) supported production of ^{210}Pb in the sediments and the flux of ^{210}Pb (or the activity at the sediment-water interface, which amounts to the same).

Model (2). In addition to model (1), there is diffusive mixing, but no nonlocal exchange. The model consists of only one layer with a flux boundary (B1) and a no-gradient boundary at depth (B5). Parameters to be estimated by least squares fit are the supported production of ^{210}Pb, the flux of ^{210}Pb and the bioturbation coefficient Db.

Model (3). Model (2) is modified by injecting (nonlocally) part of the flux at a depth L. There are two layers to be considered, ranging from [O– L] and from [L–∞] (four integration constants), with equal Db and w. Part of the flux appears at the interface between the two layers. Boundary conditions are the flux boundary at the upper interface (B1), the no-gradient boundary (B5) at $x = \infty$, and between both layers, continuity of flux

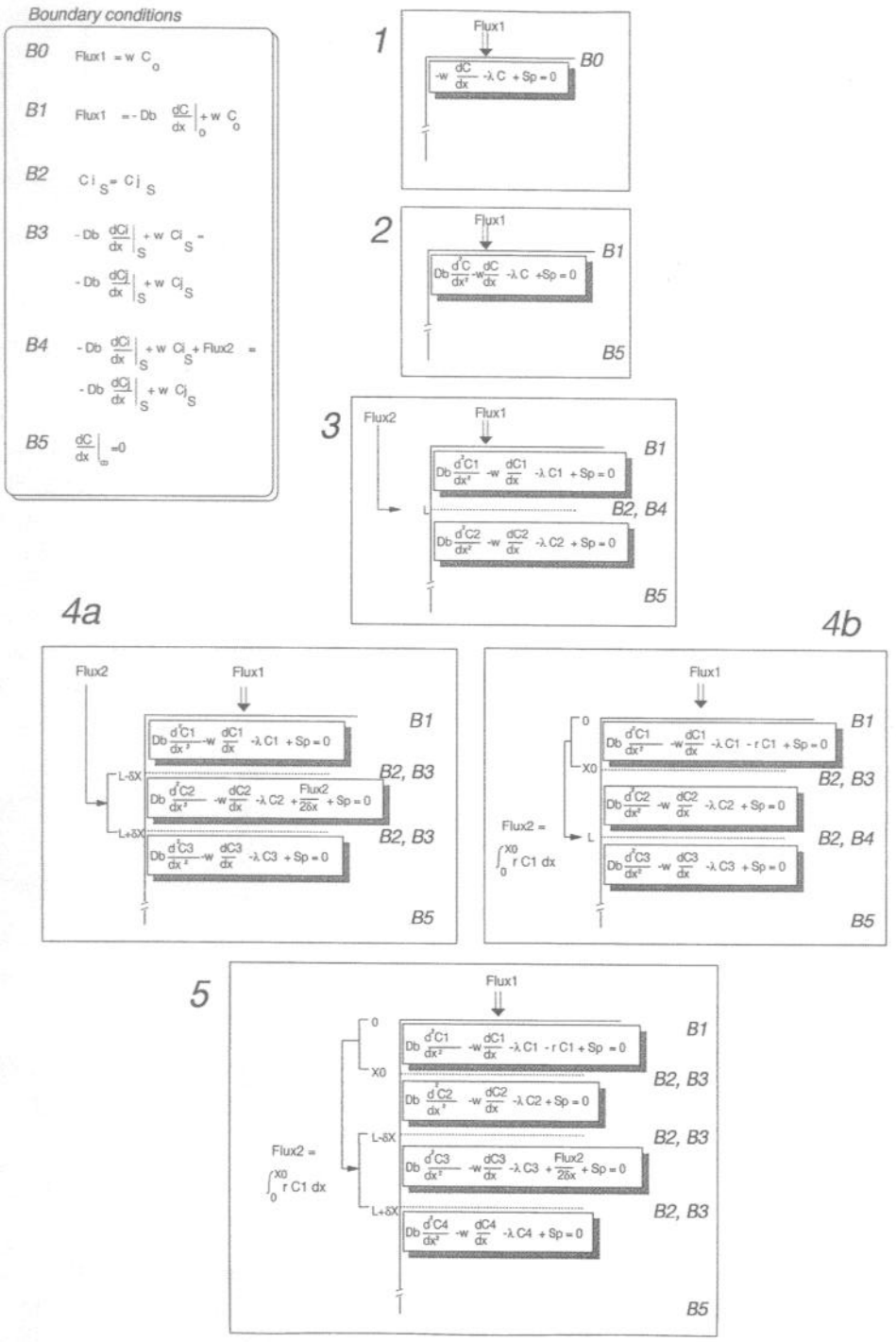

Figure 2. Schematic representation of the various models used. The diagenetic equations for the various layers are in the right boxes. Boundary conditions are denoted with B1, . . . B5 and are given in the panel above left (*i* and *j* apply to a layer number, 0 indicates the sediment surface, *S* is some depth in the sediment).

Table 2. Parameters that are estimated (+) or calculated (C) in the various models and the total number of parameters. The decay rate of ^{210}Pb, λ, is fixed (0.031 yr^{-1}), the sedimentation rate, w, is known (see material and methods).

	Sp	Flux_1	*Db*	Flux_2	*r*	*L*	δx	X_0	# Par
(1)	+	+							2
(2)	+	+	+						3
(3)	+	+	+	+		+			5
(4a)	+	+	+	+		+	+		6
(4b)	+	+	+	C	+	+		+	6
(5)	+	+	+	C	+	+	+	+	7

(B4) and of activity (B2). Compared to the previous model (2), this model requires two extra fitting parameters: namely the flux of ^{210}Pb that is directly injected into the sediment (Flux_2) and the depth where this injection occurs (L).

Model (4a). As in model (3), but the flux is injected into a layer with thickness $2\delta x$, centered at a depth L. It is implied that the material is egested homogeneously in this layer. The system now consists of three different layers, and 6 boundary conditions (Flux boundary at $x = 0$, no-gradient boundary at $x = \infty$ and continuity of activity and flux between layers). Compared to model (3), there is one additional parameter to fit, i.e. the thickness of the deposition area, $2\delta x$.

Model (4b). The same as in model (3), but now the flux, injected at depth L, has been derived by ingesting surficial sediment from a zone with thickness X_0. The first-order ingestion rate, r, is a constant. Compared to model (3), there are two additional parameters to fit (X_0 and r). The flux that is injected at depth L (which had to be estimated in model (3)) can be calculated by integrating the total ingestion within X_0. There are three different layers, with 6 boundary conditions (flux boundary at $x = 0$, no-gradient boundary at $x = \infty$ and continuity of activity and flux between layers). The solution of this model is given in the Appendix.

Model (5). The same as model (4b), but now the flux, derived from a zone with thickness X_0 is injected in a region centered around L of thickness $2\delta x$. This is the model that was used by Smith *et al.* (1986). There are four layers, 8 boundary conditions. Compared to the previous model (4b) this requires the estimation of one extra parameter (δx).

The various models were implemented as a FORTRAN code. When there were only one or two layers in the model, the integration constants were solved analytically from the boundary conditions. When there were more than two layers, the integration constants were considered as the unknowns of a set of linear equations, which was solved using standard numerical techniques (LU decomposition—Press *et al.,* 1987).

d. Estimating best parameter values

Adjusting the model to the observed activity-depth profiles required determination of the values of the unknown parameters (related to mixing, nonlocal exchange, flux, supported production of ^{210}Pb, see Table 2) that give the best fit between modeled and observed activities.

The model-generated activities were averaged over the sampled depth interval and compared with the ^{210}Pb measurements. The iterative Marquardt-Levenberg algorithm was used to minimize the squared residuals between these modeled and observed values (Press *et al.,* 1987). Since, in more complex nonlinear models, fitting algorithms may become trapped in local minima, several runs were performed with different initial guesses for the parameter values. With these results, the parameter values of the run with the lowest sum of squared residuals between observed and modeled values were selected.

e. Testing the significance of each model

Adding increased complexity to a model necessarily involves the introduction of new parameters that have to be estimated. Whereas this may improve the visual fit between modeled and observed data, or the coefficient of determination (r^2), the question remains whether the more complex model provides a significantly better explanation for the observed data. This can be tested with a one-tailed F-test (Sokal and Rohlf, 1995). The null hypothesis is that there is no difference in the residual variance between modeled and observed data in the more elaborate model compared to its more simple counterpart. The alternative hypothesis is then that the complex model has significantly reduced this variance. Provided that the null hypothesis is true, the property $F = (SSR_1–SSR_2)/(df_1–df_2)/(SSR_2/df_2)$ has a so-called F-distribution with $(df_1–df_2, df_2)$ degrees of freedom (Jongman *et al.,* 1987; Sokal and Rohlf, 1995). SSR_2 and SSR_1 are the sum of the squared residuals of observed and modeled values of the elaborate and simple model, respectively, and df_2 and df_1 are then the degrees of freedom (number of observations − number of parameters − 1) of the respective models. The null hypothesis is rejected when the calculated F value exceeds the critical value of this distribution.

The 'best model' for a certain station was chosen such that reducing its number of parameters (i.e. chosing the previous, less complicated, model) causes a significant increase in the sum of squared residuals. It is the minimal adequate model, with the minimal number of parameters but where no significant terms have been excluded (Crawley, 1993).

3. Results

a. Model-generated profiles

Typical activity-depth profiles generated with the various models, and the parameter values used, are displayed in Figure 3. The models were run for a tracer with the mean half-life of ^{210}Pb (22.3 yr, solid line), of ^{234}Th (24.1 d, dashed) and ^{14}C (5.6 kyr; dotted). In models 3 and 4a half of the flux is injected directly to depth. The first-order ingestion rate

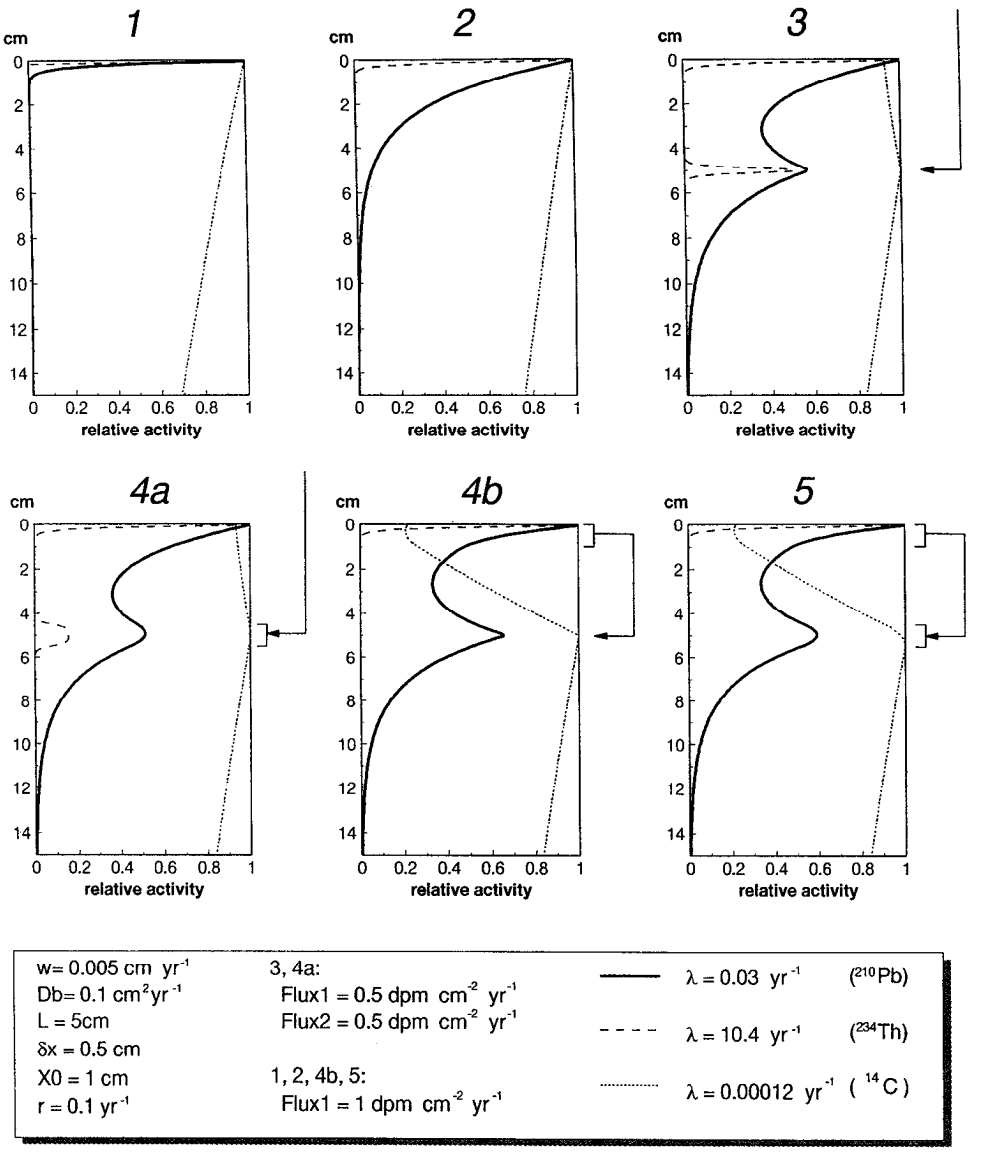

Figure 3. Example of activity-depth profiles of excess ^{210}Pb (solid line) generated with the various models explained in Figure 2. Parameter values are in the panel below. Indicated are also the profiles of a faster decaying tracer (^{234}Th, dashed line) and a more slowly decaying tracer (^{14}C, dotted line). The profiles are standardized to 1.

(r) in models 4b and 5 was chosen such that their ^{210}Pb profiles resembled ^{210}Pb profiles generated with models 3 and 4a.

Interestingly, notwithstanding the similarity among the ^{210}Pb profiles, the shorter-lived (^{234}Th) and longer-lived (^{14}C) tracers behave differently in case the flux is taken directly

from the water column compared to ingestion from the sediment surface layer. The shorter-lived tracer shows a visible peak at the egestion site in the former case, while ingestion of the upper sediment only marginally affects its activity at the egestion depth. The activity of the longer-lived tracer is distinctly more depressed in the upper layers when surface sediment ingestion occurs compared to water-column feeding. Such a tracer could also be representative for the (nearly) refractory component of the natural organic matter, and its distribution could provide an explanation for some aberrant organic carbon profiles (e.g. Brand and Shimmield, 1991) or ^{14}C profiles (e.g. Buffoni *et al.*, 1992).

As a check on the Levenberg-Marquardt algorithm we have tested whether the ^{210}Pb profile generated with model 3 could be represented with models 4a, 4b and 5. The algorithm attained a mean residual sum of squares in the order of 10^{-8} for all three models. Correspondence was achieved when the thickness of the ingestion layer (X_0) was very small (0.02 cm), and r about 3 yr^{-1} in models 4b and 5, and when the thickness of the egestion layer ($2\delta x$) was about 0.04 cm in model 5 and 4a.

In the various models we inherently assumed that, although the amount of tracer directly injected at depth could be large, the sedimentation rate remained unaltered. Such an assumption is valid for a tracer that is preferentially associated with organic matter (Wheatcroft, 1992) and is concentrated by some organism, while the amount of sediment involved in the ingestion/egestion process is small (Smith *et al.*, 1986). If, however, there is no discrimination between particles, the sedimentation rate (w) will be affected and w should change with depth (Boudreau, 1986b). Because we do not know which mode of feeding prevails, we cannot decide whether or not to make w spatially variable or the type of depth function to use. Nevertheless, we can assess its possible effect on the generated profiles. An analytical solution with spatially variable w is not easily obtained for models 4a, 4b and 5, but it can easily be included in model type 3 (water column flux injected at the interface between layers). We have performed a simulation where (in model 3) the sedimentation rate in the upper layer was set to 0, while the sedimentation rate was 5 cm kyr^{-1} in the lower layer (i.e. a preferential ingestion of 'inert' particles); the other parameters were as in Figure 3. Even in such an exaggerated simulation, the difference between the profile thus obtained and the one generated with a constant sedimentation rate was rather limited. The deviation was largest near the sediment-water interface (5%), and the average deviation was only 0.5%. Thus, at these normal oceanic sedimentation rates, spatial variation of w does not markedly affect profiles generated with model 3.

b. Modeling sediment mixing in Goban Spur sediments

We have tested which model best describes the activity versus depth profiles of ^{210}Pb in the OMEX sediments (Fig. 4). The results of the significance tests are listed in Table 3. In order not to generate activity peaks that are supported by too few data, we have restricted the depth of the nonlocal exchange zone (L) to [0–10 cm]. Below 10 cm depth, the resolution of the measurements is too limited. In all but four cases, the inclusion of a diffusive mixing coefficient does significantly improve the fit of modeled versus observed

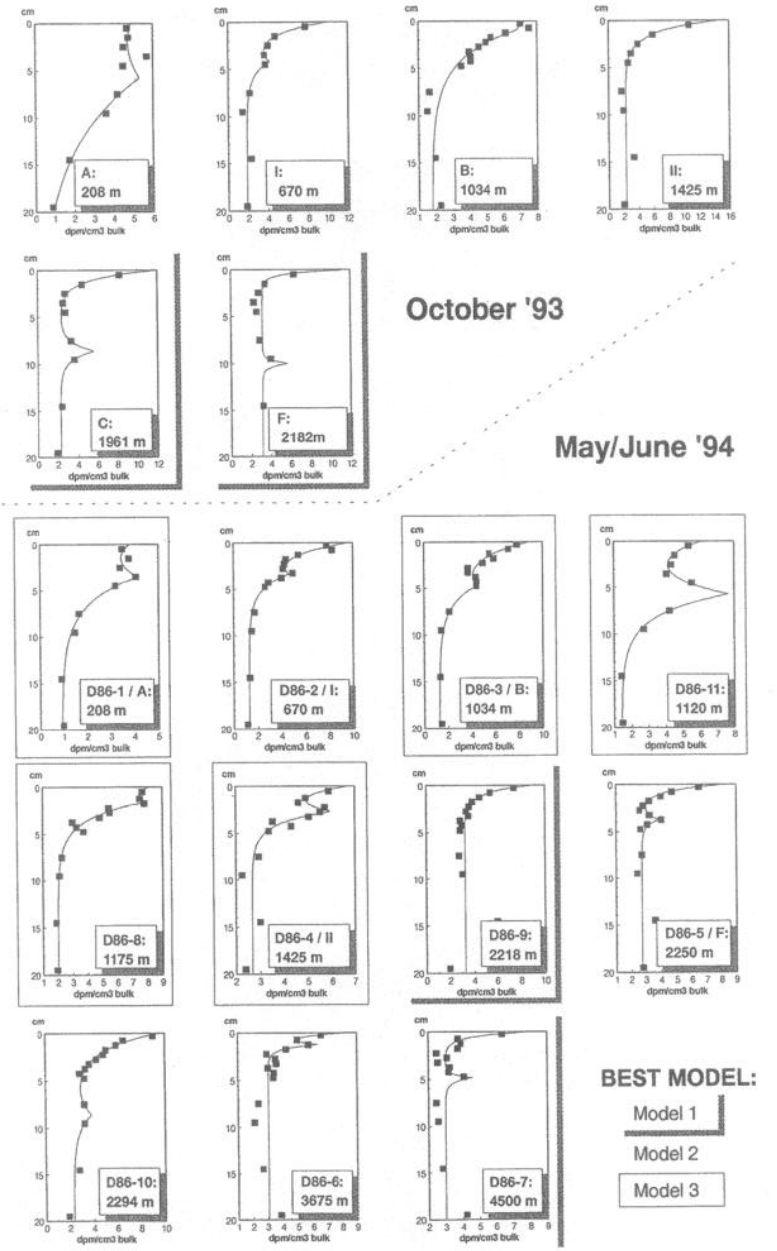

Figure 4. A comparison of measured ^{210}Pb activities and profiles generated with model 3 in OMEX sediments (see Fig. 2 for a definition of the various models). Profiles that were significantly best fitted with model 3 are in the boxes; profiles that were best fitted with model 1 are shaded below right, the other profiles were best fitted with model 2.

Table 3. Significance level of rejection of H_0; model parameters for model 3 and the bioturbation coefficient derived with model 2. The hypothesis (H_0) is that the variance between modeled and measured values is not significantly different between both models. For more information about the F-test, see text or Sokal and Rohlf (1995) or Jongman *et al.* (1987).

		Hypothesis testing			Model 3 parameters					Model 2
Station	Depth	$H_0(1/2)$	$H_0(2/3)$	Best model	*Sp*	$Flux_1$	*Db*	$Flux_2$	*L*	*Db*
A	208	**	NS	2	.00	0.29	2.10	1.95	5.8	7.87
D86-01	208	**	*	3	.03	0.13	0.25	0.46	3.5	3.59
I	670	**	NS	2	.06	0.34	0.06	0.16	4.2	0.16
D86-02	670	***	NS	2	.04	0.39	0.08	0.23	3.4	0.30
B	1034	***	NS	2	.06	0.25	0.27	0.37	1.0	0.37
D86-03	1034	***	*	3	.04	0.48	0.14	0.32	4.7	0.53
D86-11	1120	**	*	3	.04	0.27	0.15	0.81	5.8	7.14
D86-08	1175	***	*	3	.06	0.17	0.10	0.45	1.6	0.32
II	1425	**	NS	2	.07	0.43	0.04	0.04	2.0	0.05
D86-04	1425	***	*	3	.08	0.13	0.05	0.23	2.7	0.81
C	1961	NS	NS	1	.07	0.29	0.03	0.20	8.6	0.02
F	2182	NS	NS	1	.10	0.11	0.004	0.06	10.0	0.002
D86-09	2218	NS	NS	1	.10	0.12	0.01	0.02	1.1	0.02
D86-05	2250	**	NS	2	.09	0.12	0.01	0.04	3.7	0.01
D86-10	2294	***	NS	2	.07	0.41	0.10	0.16	8.6	0.08
D86-06	3675	**	NS	2	.09	0.07	0.005	0.08	1.2	0.07
D86-07	4500	NS	NS	1	.09	0.08	0.005	0.04	4.8	0.003

***: $p > 0.999$; **: p in [0.99–0.999]; *: p in [0.95–0.99]; (the more complex model is significantly better). NS: not significantly rejected; (i.e. the more complex model does not significantly improve the fit). All other combinations are not significant anywhere.

Sp (Supported production) is in dpm cm^{-3} yr^{-1}, $Flux_1$ (flux to the sediment-water interface) and $Flux_2$ (flux that is directly injected (are in dpm cm^{-2} yr^{-1}, *Db* is in cm^2/yr^{-1}, *L* is in cm.

activities in the upper 20 cm of sediment. Results are not significantly better at stations C, F, D86-07 and D86-09, where total activity drops to supported levels in a few centimeters (mixing is very small). Additionally, at station D86-07, scatter in the observed values resulted in a poor fit for all models. For the other stations, the profiles suggest that the sediments are mixed over the entire depth interval containing excess ^{210}Pb. In five cases the fit between modeled and observed activities is significantly better when part of the flux is injected at a certain depth in the sediment (model 3 compared to model 2). They are stations D86-01, D86-03, D86-11, D86-08 and D86-04 (all sampled in May/June 1994, see Table 1). The fits produced with model 3 for all stations are illustrated in Figure 4. The inclusion of more parameters (models 4a, 4b or 5) did not result in significant improvements.

We have used model (3) to generate bioturbation coefficients in the OMEX sediments (with the effects of nonlocal exchange explicitly accounted for) and to test the relative importance of nonlocal exchange in sediment mixing. The latter can simply be done by comparing the flux that is directly injected into the sediment with the total flux (injection

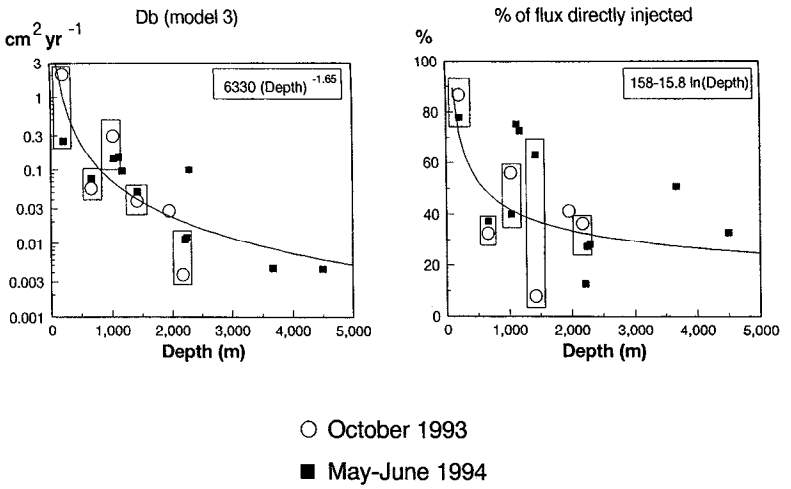

Figure 5. Estimated bioturbation coefficient and the % of the flux directly injected into the sediment (using model 3) versus water depth. The rectangles enclose stations sampled twice; the best-fit lines are indicated.

flux + flux incorporated at the sediment surface). The results are depicted in (Fig. 5). Except for the shallowest station (A/D86-01), there is reasonably good correspondence between model-derived bioturbation rates from both seasons. Bioturbation coefficients decrease with water depth. Similarly, the estimated contribution of nonlocal exchange phenomena to total sediment mixing shows reasonable correspondence between seasons, except for one station (II/D86-4) at 1425 m depth, where direct injection of the flux in May–June was estimated to be substantially higher than in October. On average, the importance of nonlocal exchange decreases with water depth; the estimated amount of flux directly injected varies from 6 to 86%. It should be realized however that the predicted subsurface maxima, for some of the deeper stations, are supported by very few data.

4. Discussion

We have described a set of models that allows us to evaluate systematically the importance of various mixing processes acting on marine sediments. Whereas it is usually left to the investigator to decide which processes are important, the one-tailed F-test (Sokal and Rohlf, 1995) provides a way of testing whether adding more complexity better explains the available data. As such, including sophisticated detail, not supported by the resolution of the dataset can be prevented. At four sites along the OMEX transect (depth from 1960–4500 m), diffusive sediment mixing is so low that the inclusion of a bioturbation coefficient does not lead to a significantly better fit. One may thus conclude that, at these sites, the effect of organisms (assuming they are responsible for diffusive mixing) on ^{210}Pb profiles in the upper 20 cm of sediment is marginal. On the other hand, the ^{210}Pb profiles of five stations from the shallower part of the transect (208–1425 m) are fitted

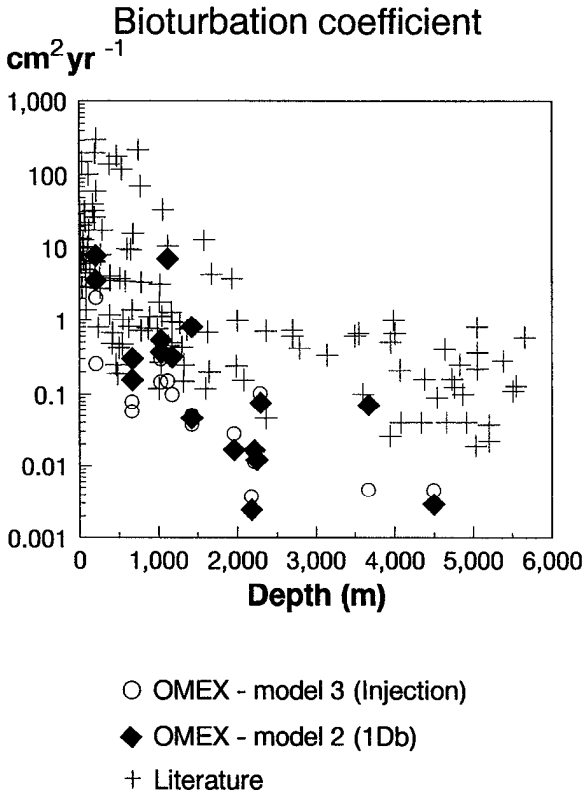

Figure 6. Excess ^{210}Pb-based bioturbation coefficient (using model 2 and 3) of the OMEX sites compared to literature data (Middelburg *et al.*, 1996).

significantly better when direct injection of part of the flux at depth in the sediment is included. The data available do not support adding more detail, however, and both the inclusion of ingestion from a finite-thickness sediment layer near the surface or egestion in a finite-thickness layer at depth in the model do not provide significantly better fits. Nevertheless, the results indicate that mixing activity on a larger scale than inherent to diffusion affects fundamentally the observed profiles of ^{210}Pb at these shallow depths in the OMEX region.

There is a three order of magnitude difference in the mixing activity along the transect, and the estimated bioturbation coefficients decrease with depth (Fig. 5), in agreement with observed decrease of the benthic biomass along the same transect (Heip *et al.*, 1995). Compared to values from the literature (Middelburg *et al.*, 1996), the bioturbation coefficients (based on the classical model 2) in the shallow regions of the OMEX area are well within ranges found at similar depths elsewhere in the oceans (Fig. 6). Mixing activity at the deeper parts is, however, clearly smaller than one would expect based on literature values. Total ^{210}Pb activities drop to the (estimated) supported level in a few centimeters at

these deep stations (Fig. 4), and this results in estimated bioturbation coefficients on the order of $10^{-3} - 10^{-1}$ cm^2 yr^{-1}. Similarly, there seems to be a decrease in the relative importance of nonlocal exchange processes with water depth (Fig. 5), which is consistent with an increased dominance of smaller benthic animals with water depth at these sites (Heip *et al.,* 1995) and, indeed, in general (Thiel, 1975).

Because of the relatively low decay rate of ^{210}Pb, its inventory is sufficiently large to dampen seasonal variability in its flux. Hence one should expect the ^{210}Pb sediment profiles to reflect a long-term average and to be relatively stationary in time. In the OMEX sediments, the bioturbation coefficient, derived from sampling the same station, at different times of the year, is more or less comparable (Fig. 5-left) and deviations probably reflect small-scale spatial differences, rather than temporal variations. Similarly, the magnitude of nonlocal exchange versus total mixing for the two cruises are comparable (Fig. 5-right); however, there is a large discrepancy for station (D86-4, II) at 1425 m depth during the two cruises. This difference is also apparent in oxygen microprofiles (Helder and Epping, 1995), where a subsurface maximum was present in May–June, at the same sediment depth as the subsurface ^{210}Pb peak (Fig. 7). Apparently, the box corer had struck a system of burrows then. Despite these differences in nonlocal exchange rates for this station, there is a strong similarity in predicted bioturbation coefficients based on model 3, whereas those based on the one-Db model (model 2) are almost by a factor of 20 different (Table 3).

There is a set of alternative models that have been applied when one-*Db* equations have failed to reproduce activity-versus-depth profiles. These are the so-called depth-zoned bioturbation models (Benninger *et al.,* 1979). In these, the sediment is subdivided in two or more layers where the simple advection-diffusion-decay equation applies, but sediment mixing in deeper zones may be several orders of magnitude smaller than in the surficial layer (e.g. Silverberg *et al.,* 1986; Aller and DeMaster, 1984; Li *et al.,* 1985; Kim and Burnett, 1988). In the OMEX area, at least three stations (A, D86-1 and D86-8, Fig. 4) comply with a two-layer bioturbation model, with high mixing on top. We have tried to apply these models to the OMEX stations, but the fitting algorithm came up with an infinitely large bioturbation coefficient in the upper layer (because of the observed small maximum at depth). Moreover, it is unclear what physical or biological processes could be responsible for such high mixing rates. In other OMEX stations there is a pronounced subsurface maximum in activity (e.g. in station D86-11 or D86-5), that cannot be reproduced by (a combination of) diffusive mixing processes. Similar profiles have been described by many other authors (e.g. Nozaki *et al.,* 1977; Stordal *et al.,* 1985; Kershaw, 1985; Jahnke *et al.,* 1986; Smith *et al.,* 1986; Buesseler and Sholkovitz, 1987; Anderson *et al.,* 1988; Brand and Shimmield, 1991; Tanaka *et al.,* 1991; Thomson *et al.,* 1993; Legeleux *et al.,* 1994); these too are probably best fitted with one of the nonlocal exchange models.

Some investigators have found evidence for an apparent low-bioturbation layer on top of the sediment (Li *et al.,* 1985; Legeleux *et al.,* 1994). Such profiles were modeled by Li *et al.* (1985) and Legeleux *et al.* (1994) using a three-layer bioturbation model with the

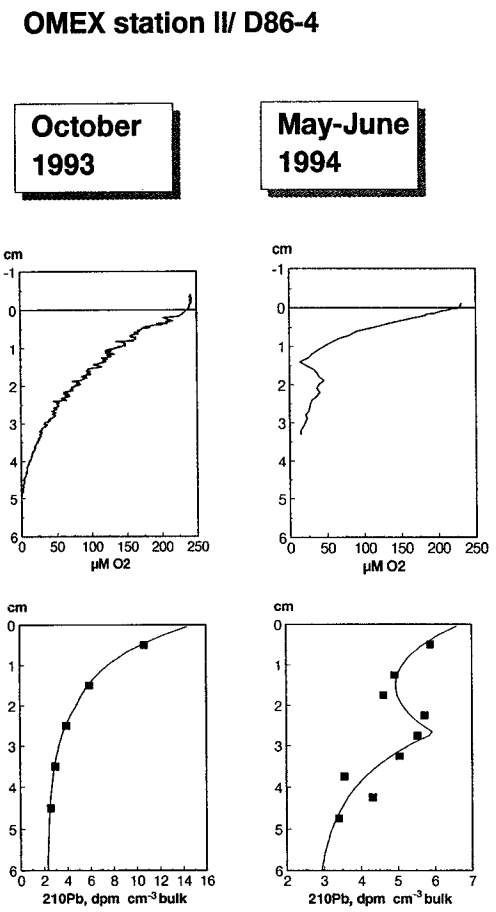

Figure 7. A comparison of the oxygen profiles and the ^{210}Pb profiles in OMEX station II/D86-4 (1425 m) during the two cruises.

subsurface sediments being mixed more rapidly than the over- or underlying sediment. Because of the aberrant nature of some of these ^{210}Pb profiles (the stations KTB-09, KTB-11, KTB-14 and KTB-16 in Legeleux *et al.,* 1994), we tested whether our set of models could reproduce them. The results for two stations are depicted in Figure 8; the other two stations gave similar results. All these profiles fitted well with at least one of the nonlocal exchange models. For core KTB-16, model 4b is significantly the best model, whereas for the three other cores, model 4a is significantly the best. Since they do not belong to the same family of models, it is not possible to test whether the nonlocal exchange models (4a and 4b), which require estimation of 5 parameters, are better than the models of Legeleux *et al.* (1994) with 6 parameters (a flux or activity upper boundary, three mixing coefficients and the depth of the interface between layers 1, 2 and between 2, 3). Neither does the drop below detection limits of shorter-lived tracers such as ^{234}Th in a few

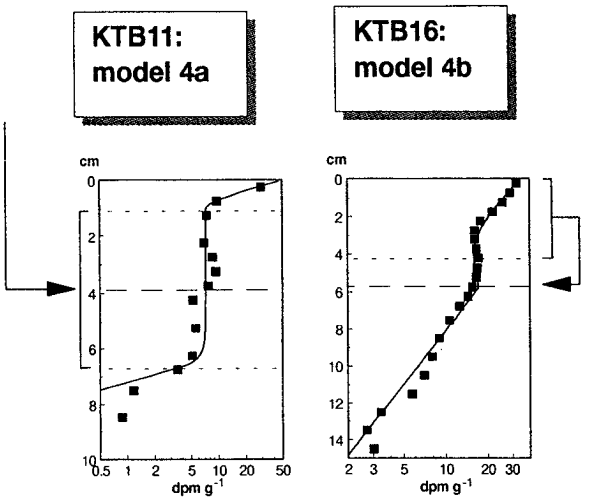

Figure 8. Model-generated profiles and measured excess ^{210}Pb activities of two stations reported in Legeleux *et al.* (1994). For the model we assumed a constant dry weight/wet volume conversion (0.5). Model parameters were for KTB11: L = 3.8 cm, δx = 2.8 cm, Flux1 = 0.31 dpm cm^{-2} yr^{-1}, Flux2 = 0.63 dpm cm^{-2} yr^{-1}, Db = 0.0044 cm^2 yr^{-1}; for KTB16: L = 5.7 cm, r = 0.03 yr^{-1}, X_0 = 4.3 cm, Flux1 = 2.95 dpm cm^{-2} yr^{-1}, Db = 0.53 cm^2 yr^{-1}.

centimeters (Legeleux *et al.*, 1994) invalidate the nonlocal exchange models. We have calculated that at station KTB-11 only 3.5% of the interface activity of ^{234}Th would be present in the egestion layer, compared to 18% for ^{210}Pb (model 4a). For station KTB16 (model 4b), the ratio would be 0.2% for ^{234}Th, compared to 50% for ^{210}Pb. As a possible cause for high rates of mixing in the intermediate layer, Legeleux *et al.* (1994) suggested the occurrence of burrowing macrofauna, living in the subsurface sediments. These animals may also be responsible for the nonlocal exchange phenomena. Hence, the set of nonlocal exchange models are at least competitive with the multi-layer bioturbation models for this type of data. Profiles that at first sight lend themselves to the multi-layer bioturbation model can with equal ease be generated by nonlocal exchange phenomena.

The difference in behavior between long- and short-lived tracers with respect to nonlocal exchange phenomena (Fig. 3) may explain why, in the same sediment, some tracers clearly exhibit subsurface peaks, while others tend to conform to more typical diffusion-like profiles. There is also a large difference in model-generated profiles between tracers with strongly different half-lives if sediment is either ingested from the surface layer (models 4b, 5) or when part of the flux from the water column is injected at depth (models 3, 4a; Fig. 3). Furthermore, profiles generated with the multi-layer bioturbation models will be much different for such a set of tracers. Hence a comparison between profiles of tracers with half-lives several orders of magnitude different could provide insight into which model is best suited to explain any set of data.

In summary we have investigated the nature and quantified the various modes of

sediment mixing processes in ocean margin sediments in the OMEX area (NE Atlantic), and we have explored some of the properties and applicabilities of nonlocal exchange models. Ultimately such processes can be incorporated into coupled models of early diagenesis (Boudreau, 1996; Soetaert *et al.,* 1996), and the impact of various modes of mixing on the diagenetic pathways examined.

Acknowledgments. The model and data discussed in this paper were developed and obtained in the framework of the Ocean Margin EXchange (OMEX) project, financed by the MAST programme of the Commission of European communities (MAS2-CT93-0069 through grants to C. Heip, T. van Weering and W. Helder). Modeling was performed by K.S., P.H., J.M., C.H.; sediment samples and ^{210}Pb profiles were obtained by H.d.S. and T.v.W.; O_2 profiles were measured by E.E. and W.H. Thanks to Dr. Boudreau and an anonymous reviewer for constructive comments. This is paper number 2154 from the NIOO-CEMO. The fitting routines and statistical testing for the set of models were implemented in FORTRAN and are available upon request.

APPENDIX

Equations of Model 4b

The activity in the various layers (Fig. 2) is given by:

$$C_1 = A_1 \cdot e^{\theta_{1a}x} + E_1 \cdot e^{\theta_{2a}x} + \frac{Sp}{\lambda + r}$$

$$C_2 = A_2 \cdot e^{\theta_1 x} + E_2 \cdot e^{\theta_2 x} + \frac{Sp}{\lambda}$$

$$C_3 = A_3 \cdot e^{\theta_1 x} + E_3 \cdot e^{\theta_2 x} + \frac{Sp}{\lambda}$$

where

$$\theta_1 = \frac{w - \sqrt{w^2 + 4\lambda Db}}{2Db}, \quad \theta_{1a} = \frac{w - \sqrt{w^2 + 4(\lambda + r)Db}}{2Db}, \quad \theta_2 = \frac{w + \sqrt{w^2 + 4\lambda Db}}{2Db},$$

$$\theta_{2a} = \frac{w + \sqrt{w^2 + 4(\lambda + r)Db}}{2Db}$$

The integration constants A_i and E_i ($i = 1, 2, 3$) are calculated from the boundary equations (B1 . . . B5; Fig. 2):

(1) Flux boundary (B1)

$$\text{Flux}_1 - w \cdot \frac{Sp}{\lambda + r} = (w - Db \cdot \theta_{1a}) \cdot A_1 + (w - Db \cdot \theta_{2a}) \cdot E_1$$

(2) Continuity of concentration at X_0 (B2)

$$\frac{Sp}{\lambda} - \frac{Sp}{\lambda + r} = e^{\theta_{1a}X_0} \cdot A_1 + e^{\theta_{2a}X_0} \cdot E_1 - e^{\theta_1 X_0} \cdot A_2 - e^{\theta_2 X_0} \cdot E_2$$

(3) Continuity of flux at X_0 (B3)

$$w \cdot \frac{Sp}{\lambda} - w \cdot \frac{Sp}{\lambda + r} = +(w - Db\theta_{1a}) \cdot e^{\theta_{1a}X_0} \cdot A_1 + (w - Db\theta_{2a})e^{\theta_{2a}X_0} \cdot E_1$$
$$-(w - Db\theta_1)e^{\theta_1 X_0} \cdot A_2 - (w - Db\theta_2)e^{\theta_2 X_0} \cdot E_2$$

(4) Continuity of concentration at L (B2)

$$0 = e^{\theta_1 L} \cdot A_2 + e^{\theta_2 L} \cdot E_2 - e^{\theta_1 L} \cdot A_3 - e^{\theta_2 L} \cdot E_3$$

(5) Continuity of flux at L (B4)

$$0 = \frac{r \cdot (e^{\theta_{1a}X_0} - 1)}{\theta_{1a}} \cdot A_1 + \frac{r \cdot (e^{\theta_{2a}X_0} - 1)}{\theta_{2a}} \cdot E_1 + (w - Db\theta_1) \cdot e^{\theta_1 L} \cdot A_2$$
$$+ (w - Db\theta_2)e^{\theta_2 L} \cdot E_2 - (w - Db\theta_1)e^{\theta_1 L} \cdot A_3 - (w - Db\theta_2)e^{\theta_2 L} \cdot E_3$$

(6) Gradient condition at infinity (B5)

$$0 = E_3$$

REFERENCES

Aller, R. C. 1990. Bioturbation and manganese cycling in hemipelagic sediments. Phil. Trans. R. Soc. Lond, *331,* 51–68.

Aller, R. C. and D. J. DeMaster. 1984. Estimates of particle flux and reworking at the deep-sea floor using $^{234}Th/^{238}U$ disequilibrium. Earth Planet. Sci. Lett., *67,* 308–318.

Anderson, R. F., R. F. Bopp, K. O. Buesseler and P. E. Biscaye. 1988. Mixing of particles and organic constituents in sediments from the continental shelf and slope off Cape Cod: SEEP-I results. Cont. Shelf Res., *8,* 925–946.

Anderson, R. F., G. T. Rowe, P. F. Kemp, S. Trumbore and P. E. Biscaye. 1994. Carbon budget for the mid-slope depocenter of the Middle Atlantic Bight, *in* Shelf Edge Exchange Processes in the Southern Middle Atlantic Bight: SEEP-II, P. E. Biscaye, G. T. Csanady, P. G. Falkowski and J. J. Walsh, eds., Pergamon, Oxford. Deep-Sea Res. II, *41(2/3),* 669–703.

Benninger, L. K., R. C. Aller, J. K. Cochran and K. K. Turekian. 1979. Effects of biological sediment mixing on the ^{210}Pb chronology and trace metal distribution in a Long Island Sound sediment core. Earth Planet. Sci. Lett., *43,* 241–259.

Berner, R. A. 1980. Early Diagenesis—A Theoretical Approach, Princeton University Press, Princeton, NJ, 241 pp.

Boudreau, B. P. 1986a. Mathematics of tracer mixing in sediments: I. Spatially-dependent, diffusive mixing. Am. J. Sci., *286,* 161–198.

—— 1986b. Mathematics of tracer mixing in sediments: II. Non-local mixing and biological conveyor-belt phenomena. Am. J. Sci., *286,* 199–238.

—— 1994. Is burial velocity a master parameter for bioturbation? Geochim. Cosmochim. Acta, *58,* 1243–1249.

—— 1996. A method-of-lines code for carbon and nutrient diagenesis in aquatic sediments. Comput. Geosc., *22,* 479–496.

Boudreau, B. P. and D. M. Imboden. 1987. Mathematics of tracer mixing in sediments: III. The theory of nonlocal mixing within sediments. Am. J. Sci., *287,* 693–719.

Brand, T. and G. Shimmield. 1991. The use of ^{210}Pb as an indicator of biological processes affecting the flux and sediment geochemistry of organic carbon in the NE Atlantic, *in* Radionuclides in the Study of Marine Processes, P. J. Kershaw and D. S. Woodhead, eds., Elsevier, London, 222–233.

Buesseler, K. O. and R. Sholkovitz. 1987. The geochemistry of fallout plutonium in the North Atlantic: I. Pore water study in shelf, slope and deep-sea sediments. Geochim. Cosmochim. Acta, *51,* 2605–2622.

Buffoni, G., R. Delfanti and C. Papucci. 1992. Accumulation rates and mixing processes in near-surface North Atlantic sediments: Evidence from C-14 and Pu-239, 240 downcore profiles. Mar. Geol., *109,* 159–170.

Crawley, M. J. 1993. GLIM for Ecologists, *in* Methods in Ecology, Blackwell Scientific Publications, London. 379 pp.

DeMaster, D. J., R. H. Pope, L. A. Levin and N. E. Blair. 1994. Biological mixing intensity and rates of organic carbon accumulation in North Carolina slope sediments. Deep-Sea Res., *41,* 735–753.

Heip, C., E. Flach, J. Vanaverbeke, M. Lavaleye and A. Sandee. 1995. Benthic community and species diversity gradients. OMEX 2nd Annual Report, E105–E117.

Helder, W. and E. Epping. 1995. Mineralization of organic matter along a transect in the Goban Spur area (Celtic Sea). OMEX 2nd Annual Report, E93–E103.

Jahnke, R. A., S. R. Emerson, J. K. Cochran and D. J. Hirschberg. 1986. Fine scale distributions of porosity and particulate excess ^{210}Pb, organic carbon and $CaCO_3$ in surface sediments of the deep equatorial Pacific. Earth Planet. Sci. Lett., *77,* 59–69.

Jongman, R. H. G., C. J. F. ter Braak and O. F. R. van Tongeren. 1987. Data analysis in community and landscape ecology. Pudoc, Wageningen, 299 pp.

Kershaw, P. J. 1985. ^{14}C and ^{210}Pb in NE Atlantic sediments: evidence of biological reworking in the context of radioactive waste disposal. J. Environ. Radioact., *2,* 115–134.

Kim, K. H. and W. C. Burnett. 1988. Accumulation and biological mixing of Peru Margin sediments. Mar. Geol., *80,* 181–194.

Legeleux, F., J-L. Reyss and S. Schmidt. 1994. Particle mixing rates in sediments of the northeast tropical Atlantic: evidence from $^{210}Pb_{xs}$, ^{137}Cs, $^{228}Th_{xs}$ downcore distributions. Earth Planet. Sci. Lett., *128,* 545–562.

Li, W. Q., N. L. Guinasso, K. H. Cole, M. D. Richardson, J. W. Johnson and D. R. Schink. 1985. Radionuclides as indicators of sedimentary processes in abyssal Caribbean sediments. Mar. Geol., *68,* 187–204.

Middelburg, J. J., K. Soetaert and P. M. J. Herman. 1996. Empirical relationships for use in global diagenetic models. Deep-Sea Res., (in press).

Nittrouer, C. A., D. J. DeMaster, B. A. McKee, N. H. Cutshall and I. L. Larsen. 1983. The effect of sediment mixing on Pb-210 accumulation rates for the Washington shelf. Mar. Geol., *54,* 201–221.

Nozaki, Y., J. K. Cochran, K. K. Turekian and G. Keller. 1977. Radiocarbon and ^{210}Pb distribution in submersible-taken deep-sea cores from project FAMOUS. Earth Planet. Sci. Lett., *34,* 167–173.

Press, W. H., B. P. Flannery, S. A. Teukolsky and W. T. Vetterling. 1987. Numerical Recipes, The Art of Scientific Computing, Cambridge University Press, Cambridge, 818 pp.

Silverberg, N., H. V. Nguyen, G. Delibrias, M. Koide, B. Sundby, Y. Yokoyama and R. Chesselet. 1986. Radionuclide profiles, sedimentation rates, and bioturbation in modern sediments of the Laurentian Trough, Gulf of St. Lawrence. Oceanol. Acta, *9,* 285–290.

Smith, J. N., B. P. Boudreau and V. Noshkin. 1986/1987. Plutonium and ^{210}Pb distributions in northeast Atlantic sediments: subsurface anomalies caused by non-local mixing. Earth Planet. Sci. Lett., *81,* 15–28.

Soetaert, K., P. M. J. Herman and J. J. Middelburg. 1996. A model of early diagenetic processes from the shelf to abyssal depths. Geochim. Cosmochim. Acta, *60,* 1019–1040.

Sokal, R. R. and F. J. Rohlf. 1995. Biometry, The Principles and Practice of Statistics in Biological Research, 3rd ed. Freeman, New York, 887 pp.

Stordal, M. C., J. W. Johnson, N. L. Guinasso and D. R. Schink. 1985. Quantitative evaluation of bioturbation rates in deep ocean sediments. II. Comparison of rates determined by ^{210}Pb and ^{239,240}Pu. Mar. Chem., *17,* 99–114.

Tanaka, N., K. K. Turekian and D. M. Rye. 1991. The radiocarbon, δ^{13}C, ^{210}Pb, and ^{137}Cs record in box cores from the continental margin of the middle Atlantic Bight. Am. J. Sci., *291,* 90–105.

Thiel, H. 1975. The size structure of the deep-sea benthos. Int. Revue ges. Hydrobiol., *60,* 575–606.

Thomson, J., S. Colley, R. Anderson, G. T. Cook and A. B. MacKenzie. 1993. ^{210}Pb in the sediments and water column of the Northeast Atlantic from 47 to 59N along 20W. Earth Planet. Sci. Lett., *115,* 75–87.

van Weering, T. C. E., G. W. Berger and J. Kalf. 1987. Recent sediment accumulation in the Skagerrak, northeast North Sea. Neth. J. Sea Res., *21,* 177–189.

van Weering, T. C. E. and H. de Stigter. 1995. Recent sediments, boundary layer dynamics and sediment accumulation at the Goban Spur margin. OMEX 2nd Annual Report, E15–E28.

Wheatcroft, R. A. 1992. Experimental tests for particle size-dependent bioturbation in the deep ocean. Limnol. Oceanogr., *37,* 90–104.

Received: *7 December, 1995;* revised: *6 June, 1996.*